

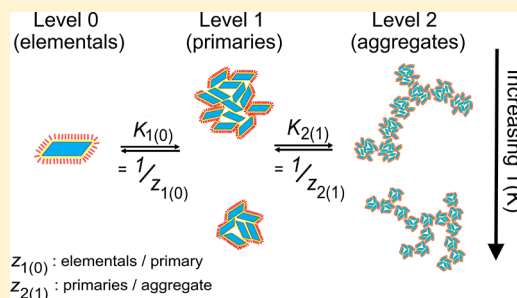
Thermodynamics of Hierarchical Aggregation in Pigment Dispersions

 Kabir Rishi,¹ Andrew Mulderig, Gregory Beaucage,^{2*} Karsten Vogtt,¹ and Hanqiu Jiang

Chemical and Materials Engineering, College of Engineering & Applied Sciences, University of Cincinnati, 2901 Woodside Drive, Cincinnati, Ohio 45221-0012, United States

Supporting Information

ABSTRACT: Many commercially and industrially important materials aggregate to form nanoscale mass-fractal structures. Unlike hard aggregates such as fumed silica, aqueous pigment-based inks consist of weakly bound nanoparticles stabilized by a surfactant. These soft aggregates can easily break apart and re-form balancing mixing energy and the reduction in surface energy with clustering or aggregation. Rapid thermal motion of small elemental crystallites leads to dense clusters or primary particles. The larger primary particles have slower thermal motion and aggregate into ramified mass fractals to form a dual-level hierarchical structure. It is proposed that the hierarchical structure relies on subtle and competitive equilibria between the different hierarchical structural levels. A new hierarchical thermodynamics model by Vogtt is used. Pigment yellow 14 and pigment blue 15:3 as surfactant-stabilized aqueous dispersions were employed to explore the thermodynamics of nanoparticle hierarchical equilibria. It was demonstrated that reversible nanoparticle aggregation can be described solely by the change in free energy of dissociation and the change in free energy of mixing in the context of a subunit being removed from a cluster. The hierarchical thermodynamics is dominated by the solubility of the dispersing surfactant. At the cloud point for the surfactant, primary particles approach the size of an elemental particle and the degree of aggregation becomes very large. The results indicate that subtle and reproducible control over pigment hierarchical structure and size is possible through thermal equilibration, manipulation of the surfactant properties, and elemental crystallite size.



INTRODUCTION

In some nanomaterials, such as fumed silica^{1–3} and carbon black,⁴ primary particles are fused together to form hard aggregates of effectively bound primary particles. The emergence of hierarchical networks in nanocomposites composed of these hard aggregates has been reported.⁵ In contrast, primary particles of aqueous dispersions of organic pigments stabilized by a nonionic surfactant are more weakly bound, forming soft aggregates.^{6–8} Pigment primary particles and their composing elemental crystallites can be removed via mechanical milling or random thermal motion, resulting in aggregate and particle size reduction and structural rearrangement.

Organic pigments contain elemental crystallites on the nanoscale with an extremely high surface area. These elemental particles cluster to form polycrystalline primary particles, characterized by the Sauter mean diameter (d_p) that describes the diameter of a sphere with the same volume to surface ratio as the particle.⁹ Pigment primary particles aggregate to form mass-fractal structures. Both the clustering, to form primary particles, and the further aggregation to form ramified mass fractals are subject to thermal equilibrium. Heating a pigment solution leads to changes in the degree of aggregation and in the primary particle size. Direct imaging techniques such as transmission electron microscopy and scanning electron

microscopy are used to produce micrographs of small numbers of polydisperse aggregates and agglomerates. However, large sample size is required to obtain representative values for a given sample.² Additionally, microscopy yields a two-dimensional (2-D) projection of the three-dimensional (3-D) aggregate structure. A 2-D projection cannot access structural details for fractal structures with dimensions greater than two. On the other hand, X-ray scattering (XS) techniques allow the characterization of structure across structural hierarchical levels from the crystalline structure measured at wide-angles (WAXS) to the fractal structure at small angles (SAXS) and then to the mesoscale structures observed at ultrasmall angles (USAXS).

Organic Pigments: PY14 and PB15:3. Organic pigments consist of insoluble, crystalline nanoparticles that tend to aggregate into mass-fractal structures. In this work, aqueous inks of pigment yellow 14 (PY14) and pigment blue 15:3 (PB15:3) are examined. PY14 is a diaryl azo pigment that forms bright yellow triclinic crystallites.^{10,11} PB15:3 is a copper phthalocyanine pigment that forms deep blue monoclinic crystallites.^{12,13}

Received: July 15, 2019

Revised: September 7, 2019

Published: September 12, 2019

Small-Angle Scattering. Small-angle X-ray scattering offers a statistical approach to characterize nanostructured branched fractal aggregates. The probe size in scattering experiments depends on the wavelength, λ , and the Bragg angle, θ , of the beam; for nanoscale materials, X-rays and neutrons are appropriate. For this work, there is sufficient electron density contrast between the aggregate samples and the aqueous dispersing medium so that X-ray scattering is employed. In small-angle scattering experiments, wavelength and scattering angle are expressed by the momentum transfer vector, $q = 4\pi \sin \theta / \lambda$, which can be directly related to the Bragg spacing, $d = 2\pi / q$.^{2,3,9,14–16} The momentum transfer vector, q , typically has units of \AA^{-1} . Therefore, small structural features will be measured at high q , while larger structures will be probed in the low- q regime. The Unified Scattering Function, shown in eq 1, is often used to fit reduced, desmeared X-ray scattering data across multiple hierarchical structural levels^{14,15}

$$I(q) = \sum_{i=1}^n G_i \exp(-q^2 R_{g,i}^2 / 3) + \exp(-q^2 R_{g,i-1}^2 / 3) B_i (q_i^*)^{-P_i},$$

$$q_i^* = q / \text{erf}(1.06q R_{g,i} / \sqrt{6})^3 \quad (1)$$

In this notation, $i = 1$ denotes the smallest structural level with higher values of “ i ” describing larger structures in the hierarchy. The Unified Scattering Function applies Guinier’s law and a power law at each structural level to characterize the sample across multiple length scales. Guinier’s law, the first term in eq 1, allows the size of the scattering particles at structural level i to be described by their radius of gyration, $R_{g,i}$. The power-law term in eq 1 describes the details of the structure. For smooth, dense particles, the power-law exponent, P_i , is 4 at hierarchical level $i = 1$. $1 \leq P_i < 3$ indicates a mass-fractal structure at hierarchical level $i = 2$. q_i^* in the Unified Scattering Function accommodates the transition between the Guinier and power-law regimes within a structural level.^{14,15} The Gaussian factor in the second term describes the transition between structural levels.

Aqueous dispersions of organic pigments are generally composed of three structural levels, the smallest being the elemental crystallites ($i = 0$), which cluster into primary particles ($i = 1$). These primary particles further assemble into mass-fractal aggregates ($i = 2$). The Unified Fit does not account for the elemental structural level $i = 0$, the size of which is obtained from WAXS measurements. For crystalline materials, the size of the crystallites that make up the primary particles as clusters can be estimated from the broadening of the diffraction peak(s) in the wide-angle X-ray scattering data according to the Scherrer equation.^{17–19} The crystallite size $t = 0.9\lambda / B \cos \theta$, where λ is the X-ray wavelength, B is the full width of the peak at half of the maximum in radians, and θ is the Bragg angle. The size-related broadening of the diffraction peak(s) combined with an assumption of the crystallite structure yields the average volume of an elemental particle in the sample, v_0 . Also, from fits of the Unified Scattering Function to small-angle scattering data, the Sauter mean diameter, d_p , of the primary particles can be calculated.^{9,20} For a power-law dependence of -4 , the hard sphere volume of a primary particle, $v_1 = \pi d_p^3 / 6$, results. The ratio of the hard sphere primary particle volume to the volume of an elemental crystallite results in the average number of elemental

crystallites in a primary particle, $z_{1(0)} = v_1 / v_0$. Additionally, the average number of primary particles in an aggregate, $z_{2(1)}$ (generally reported as z), is determined from the fits of the Unified Scattering Function.⁹ The contour volume of an aggregate is thus expressed as $v_2 = v_1 z_{2(1)}$.

Thermodynamics of Nanoparticle Assembly. For organic pigment-based inks dispersed using a nonionic surfactant, particle interactions are controlled by the surfactant and thermal motion of the particles.^{21,22} Nanoparticle aggregation involves smaller structures that assemble to form larger structures, which can be, themselves, assembled into even larger structures in the hierarchy. A thermodynamic hierarchical level is defined by a unique free-energy change for the removal of a subparticle as described in a recently developed theory by Vogtt,²³ which is summarized in this paper. The thermodynamic and structural hierarchical levels are distinct but may coincide, as in the case of the pigments studied here.

The clustering or aggregation of surfactant-stabilized pigment particles in aqueous dispersion is usually described by kinetic models that quantify the balance between thermal motion of the particles, $D \sim kT / (6\pi R)$, which is slower for larger particles due to the size-dependent Stokes drag coefficient, and the energetic benefit of reduction in surface area associated with clustering or aggregation. For the rapid motion of small particles, the bonding reaction controls aggregation and dense clusters form in reaction-limited growth or aggregation (RLA). For the slower motion of large particles, diffusion controls the growth and branched mass-fractal aggregates form in diffusion-limited aggregation (DLA). On the basis of an aggregating crystallite or primary particle, the coordination number, which is high for RLA and low for DLA, quantifies the energy change on association or dissociation.

Within the context of the kinetic models, reversible clustering and aggregation of pigment crystallites and primary particles can be considered. An equilibrated system subject to these kinetic constraints could produce dense, high-coordination number clusters or ramified mass-fractal aggregates with dramatically different coordination numbers, which would result in different free-energy changes on aggregation or clustering. This serves as the basis for a thermodynamic hierarchy, which is closely related to the structural hierarchy. Systems may exist where the structural and thermodynamic hierarchical levels do not coincide.

Following the Vogtt model,²³ we consider that elemental crystallites reversibly cluster to form 3-D primary particles. The roughly spherical primary particles can then reversibly aggregate to form secondary aggregates, which display mass-fractal structures.^{24–26}

Elemental crystallites are able to freely associate and dissociate from the primary particles with a small energy barrier. Since this process is reversible, the energy required to remove an elemental subunit is equal in magnitude to the energy required to add an elemental particle to a primary particle albeit of opposite sign. Furthermore, it is assumed that the strength of these interactions does not change with the number of elemental units in a primary particle cluster and that thermally equilibrated cluster sizes will be obtained. The change in free energy required to remove or add an elemental to the primary particle characterizes the process of clustering for the primary particle structural level. After a sufficient length of time, the free association and dissociation of elemental particles to and from the primary particles, respectively, will

result in an equilibrium number of clustered elemental particles comprising the primary particle. Similarly, higher structural levels in the hierarchy can be characterized by the change in free energy required for their assembly, and, after sufficient time has passed, an equilibrium number of primary particles comprising the aggregates can be observed. Following Vogtt's theory,²³ the unique changes in free energy for the aggregation processes for each hierarchical structural level may be determined, that is, a different energy for clustering of elemental crystallites, versus that for primary particles forming aggregates associated with differences in the coordination number per elemental or primary particle.

Using Vogtt's theory,²³ the aggregation thermodynamics for the process of removing subunits from a cluster can be quantified across the different hierarchical structural levels, as depicted in Figure 1. It is emphasized that the number of subunits in each hierarchical level is a direct consequence of the change in free energy per subunit that associates to form a cluster at a particular level. The actual structure, quantified by the mass-fractal dimension, connectivity dimension, and minimum dimension, as well as the degree of aggregation,²⁴ is a consequence of growth kinetics, which impact the coordination number and the energy of aggregation or clustering.

In the following treatment, the elemental crystallites are considered monodisperse with size determined from the

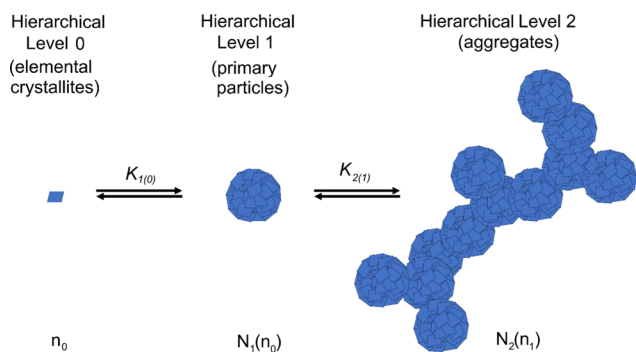


Figure 1. Cartoon illustrating the removal of subunits from hierarchical clusters of PB15:3. In this example, the material displays two structural hierarchical levels. The free energy associated with the removal of a monomeric elemental crystallite from a primary particle is characterized by an equilibrium constant, $K_{1(0)}$. Likewise, the removal of a primary particle from an aggregate can be described using the equilibrium constant, $K_{2(1)}$. Elemental particles are considered monodisperse, whereas the number distributions $N_1(n_0)$ and $N_2(n_1)$ indicate the polydispersity at the primary particle and aggregate hierarchical levels respectively.

Scherrer equation, whereas the primary particles and aggregates are considered polydisperse. This polydispersity in size is expressed as the number distribution of primary particles, $N_1(n_0)$, consisting of n_0 elemental crystallites and the number distribution of aggregates, $N_2(n_1)$, comprising n_1 primary particles. A description of the equilibrium aggregation process as depicted in Figure 1, through a conventional law of mass action, is not viable due to a myriad of dissociation pathways. However, this can be reconciled in the Vogtt approach by considering the overall change in concentration of the clusters (e.g., aggregates) as they reversibly dissociate into subunits (e.g., primary particles) while displaying a stable osmotic pressure (total number density of particles). Based on

the difference in chemical potentials for the cluster-subunit equilibrium, Vogtt²³ proposed that the free-energy change for dissociation is given by

$$\begin{aligned} \Delta G_{2(1)} &= RT \ln(N_1^T/N_2^T) = RT \ln(z_{2(1)}) \\ &= -RT \ln(K_{2(1)}) \end{aligned} \quad (2)$$

where N_1^T is the total number of primary particles and $N_2^T = \int_0^\infty N_2(n_1)dn_1$ is the total number of aggregates at a given temperature. The ratio of N_1^T to N_2^T is the number average degree of aggregation for the primary particles, $z_{2(1)}$. At the same temperature, the equilibrium constant, $K_{2(1)}$, describes the dissociation process of removal of primary particles from aggregates. Similarly, $K_{1(0)}$ describes the process of removal of elemental crystallites from primary particles. Note that the terms inside the natural log in eq 2 are flipped for the reverse reaction, i.e., aggregation or addition of subunits to clusters.

Equation 2 relies on the assumption that a steady population distribution at a given temperature has been reached. The different dissociation pathways, such as a hexameric aggregate reducing to a pentameric aggregate, can be ignored and the equilibrium between the population of aggregates and the population of primary subunits can be considered under the assumption that the energy for dissociation does not vary greatly with size of the aggregate but differs significantly from the energy to remove an elemental crystallite from a primary particle. Vogtt's theory²³ necessitates that a stable pigment dispersion be allowed enough time to equilibrate at each level in the structural hierarchy. The removal of a subunit from a cluster at thermal equilibrium dictates that the change in the number of aggregates composed of n_1 primaries through the loss of a primary particle, for instance, $dN_2(n_1)$, results in a change in the distribution of the primaries, $N_1(n_0)dn_0$, for the clusters of size n_1 under consideration. For example, the loss of a primary subunit from an octameric aggregate will lead to an increase in the number of primary particles and a decrease in the number of octamers. The principle of conservation of mass results in

$$\langle N_2(n_1)dn_1 + z_{2(1)}dN_2(n_1) \rangle_{\text{time}} = 0 \quad (3)$$

where $z_{2(1)}$ is the average number of primary particles in an aggregate. In eq 3, the average degree of aggregation, $z_{2(1)}$, is used as a constant in the second term, but other constants are possible depending on the form of the distribution, $N_2(n_1)$. The use of $z_{2(1)}$ results in an exponentially decaying aggregate size distribution such as in step-growth polymerization or worm-like micellar equilibrium. Note that the balance in eq 3 results when the changes in subunits and the resulting change in cluster size are averaged over time.

At thermal equilibrium, eq 3 can be rearranged to represent a linear differential equation, which can be solved by imposing the constraint, $N_1^T = \int_0^\infty N_2(n_1)n_1 dn_1$, where N_1^T is the total number of primary particles, which is fixed at a given temperature. It is approximated that there is no size restriction on n_1 , which shifts the integration limits from 1 to 0 for the lower limit and from n_1 to ∞ for the upper limit. This approximate relationship is more accurate for larger values of n_1 . It allows for a more concise description of the number distribution of aggregates, $N_2(n_1)$

$$N_2(n_1) = (N_1^T/z_{2(1)}^2)\exp(-n_1/z_{2(1)}) \quad (4)$$

The result in eq 4 (refer to the detailed derivation in the Appendix in the Supporting Information) can be expressed in terms of the volume fraction of the pigment in solution, $\phi = v_1 N_1^T / V$. Here, V indicates the total volume of the solution, which can be discretized into $N_{\Omega,1} = V/v_1$ 3-D primary particle size lattice sites such that

$$-n_1/z_{2(1)} = \ln(z_{2(1)}^2/\phi) + \ln(N_2(n_1)/N_{\Omega,1}) \quad (5)$$

The first term on the right side of the expression in eq 5 (refer to the detailed derivation in the Appendix in the Supporting Information), $\ln(z_{2(1)}^2/\phi)$, indicates the thermodynamic driving force for the process of removing a primary subunit from an aggregate and is used to determine the change in free energy of dissociation. The same result was derived by Cates and Candau for worm-like micelles through minimization of the thermodynamic aggregation potential.²⁷ In Cates' work, the change in the free energy of scission, $\Delta G_{sc} = RT \ln(z_{WLM(surf)}^2/\phi)$, was described, but for nanoparticle structural hierarchies in thermal equilibrium, the more intuitive term is dissociation. The second term on the right side of eq 5, $\ln(N_2(n_1)/N_{\Omega,1})$, is recognizable as a configurational (mixing) entropy, in that it describes the log of the number of occupied volume elements relative to the total number of 3-D lattice sites in the system.

The free-energy change for the removal of a primary particle from an aggregate cluster can be determined by integrating eq 5 (see Appendix in the Supporting Information) and can be expressed as the difference of the change in free energy of dissociation and mixing of a primary particle from an aggregate

$$\begin{aligned} \Delta G_{2(1)} &= RT \{ \ln(z_{2(1)}^2/\phi) + \ln(N_2^T/N_{\Omega,1}) \} \\ &= \Delta G_{2(1)}^d - \Delta G_{2(1)}^m = RT \ln(z_{2(1)}) \end{aligned} \quad (6)$$

The thermodynamics of the dissociation process at any structural level composed of subunits (i.e., $i > 0$) can be described by eq 6. For example, the free-energy change for the removal of an elemental crystallite from a primary particle cluster is $\Delta G_{1(0)} = RT \ln(z_{1(0)}) = \Delta G_{1(0)}^d - \Delta G_{1(0)}^m$. The change in free energy required to remove a primary particle from an aggregate can be quantified in terms of the change in free energy upon dissociation of the primary subunit, $\Delta G_{2(1)}^d$, and the change in free energy upon mixing of the primary subunit into the dispersing medium, $\Delta G_{2(1)}^m$. It should be noted that, although the $\ln(N_2^T/N_{\Omega,1})$ term in eq 6 suggests a mixing entropy, $\Delta G_{2(1)}^m$ is denoted as the change in free energy upon mixing to account for the possibility of enthalpic factors. Since eq 6 employs quantities that can be determined from small-angle scattering data, the calculation of $\Delta G_{2(1)}^d$, $\Delta G_{2(1)}^m$, and $\Delta G_{2(1)}$ and their associated enthalpies and entropies requires no additional experiments beyond the small-angle scattering measurement of dilute samples across a temperature series.^{23,28} Comparison between eqs 2 (last term in eq 6) and eq 6 calculated using $\Delta G_{2(1)}^d$ and $\Delta G_{2(1)}^m$ allows for a check on the Vogtt approach.

The change in the free energy of dissociation describes the difficulty to remove a subunit from a cluster, and the change in the free energy of mixing describes the change in free energy by dispersing the subunit into the medium. The difference between the change in the free energy of dissociation and the change in the free energy of mixing yields the overall change in the free energy for the removal of a subunit from a cluster at that hierarchical structural level. Positive values of $\Delta G_{i(i-1)}$

indicate that the dissociation of a subunit from the cluster is unfavorable at the structural level, $i > 0$, and suggest cluster formation. On the other hand, negative values for $\Delta G_{i(i-1)}$ suggest that subunits will spontaneously be removed from the cluster.²³

Comparison of the overall change in free energy, $\Delta G_{i(i-1)}$, between two adjacent hierarchical structural levels in thermal equilibrium across a temperature series allows the prediction of trends in aggregate structure. For example, the sample may consist of aggregates (structural level $i = 2$) of primary particles (structural level $i = 1$), which themselves consist of elemental particles (structural level $i = 0$). In this example, both $\Delta G_{1(0)}$ and $\Delta G_{2(1)}$ are positive since primary particles and aggregates, respectively, are observed. Therefore, in the temperature range where both hierarchical structural levels are observed, tradeoffs between primary particle size and aggregate size may be predicted from the changes in entropy, $\Delta S_{i(i-1)}$, at each hierarchical structural level, $i > 0$, as listed in Table 1.

Table 1. Prediction of Trends in Average Number of Subunits with Increasing Temperature (Based on the sign of the overall change in entropy for the removal of a subunit at each hierarchical structural level ($i > 0$))

	$\Delta S_{1(0)}$	$\Delta S_{2(1)}$	$z_{1(0)}$	$z_{2(1)}$	prediction at elevated temperature
I	+	+	↓	↓	elemental particles increase at the expense of aggregates and primary particles due to a decreased entropic penalty to remove a subunit
II	-	-	↑	↑	aggregates and primary particles grow at the expense of elementals due to an increased entropic penalty for removal of a subunit
III	+	-	↓	↑	aggregates grow at the expense of the primary particle size
IV	-	+	↑	↓	primary particles grow at the cost of aggregate size

In this article, Vogtt's theory of aggregation thermodynamics,²³ summarized above, was examined for the primary particle ($i = 1$) and aggregate ($i = 2$) structural levels in samples of pigment yellow 14 and pigment blue 15:3.

■ EXPERIMENTAL SECTION

Samples of pigment yellow 14 and pigment blue 15:3 were obtained in the form of aqueous inks of the organic pigments at concentrations of 1.0 wt % (dilute), 5.5 wt %, and 6.5 wt % from Sun Chemical Corporation. The densities of PY14 and PB15:3 are 1.45 and 1.62 g/cm³, respectively, from which the respective volume fractions were determined. Each organic pigment ink was dispersed in water using Triton X-100 surfactant, C₂₄H₂₂O(C₂H₄O)_m, to stabilize the dispersions. The concentration of Triton X-100 surfactant was about 1 mg/mL (1.6 mM or about 7 times the critical micelle concentration) for all samples. At this surfactant concentration, the pigment surface coverage is independent of surfactant concentration.^{21,22}

USAXS and SAXS measurements were performed on dilute samples (1.0 wt %) at temperatures ranging from 10 °C through 80 °C in increments of 10 °C. The measurements utilized beamline 9-ID-C operated by the X-ray Science Division at the Advanced Photon Source (APS) at Argonne National Laboratory.^{29,30} A momentum transfer vector, q , of $0.0001 \text{ \AA}^{-1} \leq q \leq 0.8 \text{ \AA}^{-1}$ was achieved by this combination of instruments. The SAXS and USAXS data sets were merged using the absolute scale of the USAXS measurements. Background scattering from the aqueous medium was subtracted prior to data-stitching. The instrument was operated using synchrotron radiation at 0.5904 \AA .^{29,30} The Indra, Nika, and Irena packages³¹ for

Igor Pro were employed to reduce, desmear, and merge the data sets. First, the USAXS data was reduced and the background scattering was subtracted. USAXS data was then desmeared to account for the slit smearing. SAXS data was reduced by sector-averaging the raw data and binning the reduced data into about 400 bins. For all samples, the combined SAXS and USAXS curves were fit using the Unified Scattering Function^{14,15} shown in eq 1.

Wide-angle X-ray scattering (WAXS) measurements were also performed on the beamline 9-ID-C operated by the X-ray Science Division at the Advanced Photon Source (APS) at Argonne National Laboratory. Data was obtained in the $1.5 \text{ \AA}^{-1} \leq q \leq 6 \text{ \AA}^{-1}$ regime using a WAXS detector. The WAXS data obtained for the 5.5 wt % (PY14) and 6.5 wt % (PB15:3) pigment samples was used to estimate the size of the elemental particles. A reduction in the primary particle size from SAXS observed across the temperature series indicated that the primary particles are able to break apart and re-form. This implied the presence of elemental particles. Since both pigments are crystalline, the nanocrystallite size may be estimated from the broadening of the diffraction peak(s) via the Scherrer equation.¹⁹ Instrumental broadening and strain-related broadening were shown to be insignificant by measuring macroscopic crystals. The nanoscale size of the pigment crystallites should account for most of the observed broadening of the WAXS peaks. The size of the crystallites obtained from the Scherrer equation was taken as the average diameter of an elemental particle.

RESULTS AND DISCUSSION

The fit parameters from the Unified Scattering Function characterize the sample at multiple structural levels and are listed in Tables S2 and S3 in the Supporting Information for both of the pigments investigated at different temperatures in this study. For the pigment primary particles (hierarchical level, $i = 1$), the power-law exponent, P_1 , is 4, while for the mass-fractal aggregates (hierarchical level, $i = 2$), the power-law exponent is in the range, $1 \leq P_2 < 3$.³² Since both pigments consist of soft aggregates bound by relatively weak van der Waals forces, it seems plausible that the nanoparticle aggregates would be able to break apart and re-form in thermal equilibrium. Therefore, both the removal of a particle from the aggregate (dissociation) and mixing into the dispersing medium must be considered following Vogt's theory.²³ The size of the aggregates in terms of the average number of primary particles in an aggregate (secondary particle) has been determined through the degree of aggregation, $z_{2(1)} = (G_2/G_1) + 1$.^{4,28} The observations of decreasing primary particle size and increasing aggregate size across the temperature series (following type III in Table 1) suggest that the nanoparticles of pigment yellow 14 and pigment blue 15:3 in the inks are able to rearrange in response to changes in temperature. Crystalline subunits smaller than the primary particles are observed from the Scherrer analysis for both PY14 and PB15:3. These observations support polycrystalline primary particles.

It is expected that the crystallite size should change with temperature following the Gibbs–Thomson equation; however, the kinetics of this process appears to be very slow relative to the experimental conditions since the diffraction peak breadth at about $10^\circ 2\theta$ (PY14) and $9^\circ 2\theta$ (PB15:3) remained constant over the temperature range and time of the experiment. For the purposes of this study, the crystallite size is fixed as a function of temperature. The average full width at half-maximum of about $0.17^\circ 2\theta$ and $0.21^\circ 2\theta$ corresponded to crystallite diameters of roughly 18 and 15 nm for PY14 and PB15:3, respectively. Since broadening of the WAXS peak may also arise from the instrument and from thermal broadening

within the crystal, this size was taken as a rough estimate (diffraction peaks from bulk metal crystals had negligible broadening on this instrument, indicating that there was little instrumental broadening). The crystallites of PY14 and PB15:3 were considered to be the elemental particles that cluster under the control of the surfactant to form primary particles of the pigment nanoparticles. Using this crystallite size, the average volume of an elemental particle, v_0 , of PY14 was calculated. Dividing the volume of a primary particle, v_1 , obtained from the Unified Fit parameters in eq 1 by the volume of an elemental particle gave an estimate of the average number of elemental crystallites that make up a primary particle, $z_{1(0)}$. This value is plotted by red circles in Figure 2 and can be read

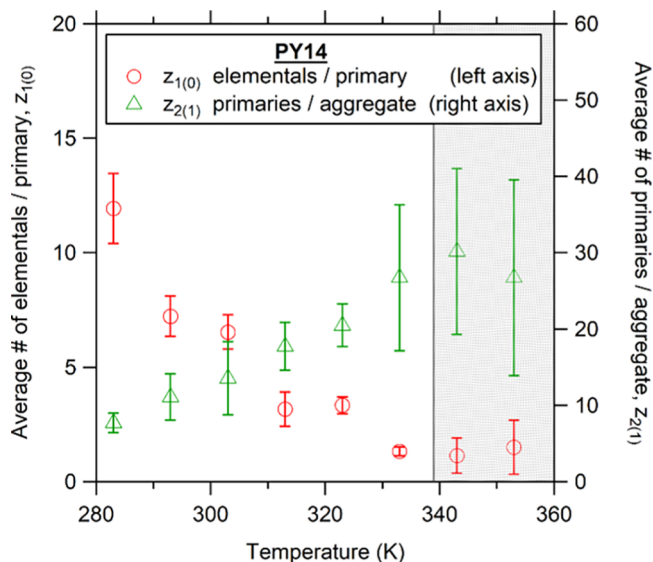


Figure 2. Thermal behavior for pigment yellow 14. The number of elemental particles in a primary particle (red circles, left axis) and the number of primary particles in an aggregate (green triangles, right axis). The vertical line corresponds to the cloud point of the surfactant (339 K), i.e., the temperature at which pigment particles phase-separate. The phase separation temperature range to the right of the gray line is shaded. For pigment blue 15:3, refer Figure S1 in the Supporting Information.

from the left axis. Additionally, the number of primary particles in an aggregate, $z_{2(1)}$, is shown by the green triangles and can be read from the right axis in Figure 2. At elevated temperatures, $z_{2(1)}$ seems to increase at the expense of $z_{1(0)}$ for PY14. Similar behavior is observed for PB15:3 as shown in Figure S1 in the Supporting Information. The gray region above 339 K indicates expected phase separation above the cloud point of the surfactant, as discussed below.

The second virial coefficient, A_2 , can be computed from the decrement in the reduced scattering intensity over a pigment concentration series as described in detail in a previous publication.³² Positive values of A_2 indicate a thermally stable dispersion. Figure 3 shows the second virial coefficient for surfactant-stabilized PY14 and PB15:3 nanoparticles as a function of inverse temperature ($1/T$) from 353 to 283 K. As the temperature increases the second virial coefficient, A_2 reduces indicating a lower critical solution temperature behavior. The critical temperature above which phase separation occurs is determined from the fits to the A_2 values in Figure 3. The critical temperatures extrapolated to $A_2 = 0$ are 340 ± 20 and 344 ± 10 K for PY14 and PB15:3,

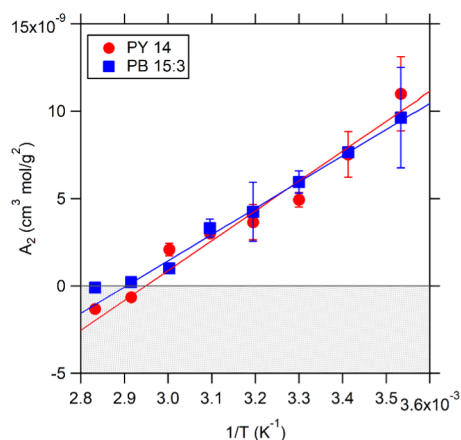


Figure 3. Variation of the second virial coefficient, A_2 , for surfactant-stabilized PY14 (solid red circles) and PB15:3 (solid blue squares) nanoparticles as a function of inverse temperature ($1/T$), across the temperature range from 283 to 353 K. The critical temperatures above which phase separation ($A_2 = 0$) occurs are 340 ± 20 and 344 ± 10 K for PY14 and PB15:3, respectively. The region associated with phase separation of pigment from solution is shaded.

respectively. The observed phase separation of pigment nanoparticles with increasing temperature can be attributed to the surfactant, Triton X-100, that becomes less miscible until bulk phase separation occurs at 339 K (66 °C). The affinity of the nonionic surfactant for the pigment surface therefore increases with temperature allowing a higher surface coverage, which is in equilibrium with the dispersed surfactant. This can mechanistically explain the decreasing clustering of elemental particles with increasing temperature. That is, particle–surfactant attraction becomes greater than particle–particle attraction as the miscibility of the surfactant decreases. The degree of aggregation increases with temperature since the reduction in primary size leads to an increase in the surface area of the primary particles so that their ability to aggregate is also impacted. So, with a decreased surfactant miscibility at higher temperatures, we see a reduction in primary size and an increase in aggregation. This could be used advantageously to control pigment structure through manipulation of the surfactant miscibility either chemically, thermally, or through the use of additives such as cosolvents.

Figure 4 shows the calculated change in free energy for dissociation of an elemental crystallite of PY14 from a primary particle of PY14 and the calculated change in free energy to mix an elemental crystallite of PY14 into the dispersing medium across the temperature range from 283 to 353 K per eq 6. The change in free energy of dissociation, $\Delta G_{1(0)}^d$, is a measure of the difficulty of removing an elemental crystallite from a primary particle. On the other hand, the change in free energy of mixing, $\Delta G_{1(0)}^m$, is the change in free energy that would be gained by an elemental crystallite mixing into the dispersing medium. Additionally, the difference between $\Delta G_{1(0)}^d$ and $\Delta G_{1(0)}^m$ represents the overall change in free energy for the process of removing an elemental crystallite from a primary particle, $\Delta G_{1(0)}$. The positive values of $\Delta G_{1(0)}$ (since $\Delta G_{1(0)}^d > \Delta G_{1(0)}^m$) across the temperature range indicate that the removal of an elemental crystallite from a primary particle cluster is unfavorable. This result is consistent with the observation of primary particles across the temperature range probed. Trends in $\Delta G_{1(0)}^d$ and $\Delta G_{1(0)}^m$ are plotted in Figure 4, and the corresponding enthalpy and entropy for dissociation

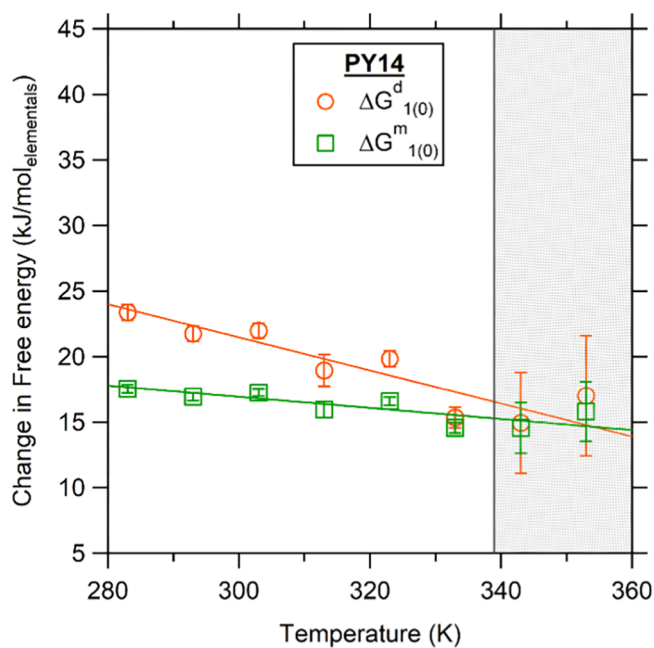


Figure 4. Change in free energy vs T for the primary particle structural level ($i = 1$) for the dilute sample of PY14 across the temperature range from 283 to 353 K. The change in free energy upon dissociation of an elemental crystallite from a primary particle (orange circles) and the change in free energy upon mixing of the elemental crystallite into the dispersing medium (green squares) are plotted. Since the change in the free energy upon dissociation is higher than the change in the free energy upon mixing, the overall change in free energy for the removal of an elemental particle from a primary particle is positive. This is consistent with the observation of primary particles. The gray line corresponds to the cloud point of the surfactant (339 K), and the values for $\Delta G_{1(0)}^d$ and $\Delta G_{1(0)}^m$ in the temperature range corresponding to phase separation of pigment from the solution (gray shaded region) are outliers to the dissociation (orange) and mixing (green) fit lines. The plot of the change in free energy vs T at this structural level ($i = 1$) for PB15:3 is shown in Figure S2 in the Supporting Information.

and mixing are listed in Table 2. The values for $\Delta G_{1(0)}^d$ and $\Delta G_{1(0)}^m$ above 339 K are outliers that do not fit the trends since the trend should not continue at temperatures above the cloud point of the Triton X-100 surfactant (339 K), as discussed above.³³ $\Delta G_{1(0)}^d > \Delta G_{1(0)}^m$ is also observed over the entire temperature range resulting in positive $\Delta G_{1(0)}$ values for PB15:3 primary particles, as shown in Figure S2 in the Supporting Information.

The change in the free energy of dissociation of a primary particle from an aggregate, $\Delta G_{2(1)}^d$, of PY14 and the change in the free energy of mixing of the primary particle into the dispersing medium, $\Delta G_{2(1)}^m$, are shown in Figure 5. Here, the dissociation and mixing approach were applied to the secondary hierarchical structural level for the dilute (1.0 wt %) sample of PY14 across the temperature range per eq 6. Trends in $\Delta G_{2(1)}^d$ and $\Delta G_{2(1)}^m$ are plotted from 283 to 343 K, and the corresponding enthalpy and entropy for dissociation and mixing are listed in Table 2. The values for $\Delta G_{2(1)}^d$ and $\Delta G_{2(1)}^m$ above 339 K are outliers that do not fit the trends due to phase separation, as discussed above. Since aggregates of primary particles were observed in USAXS/SAXS measurements, positive values of $\Delta G_{2(1)} = \Delta G_{2(1)}^d - \Delta G_{2(1)}^m$ for the removal of a primary particle from an aggregate are expected across the temperature series. Furthermore, since $z_{2(1)}$ was

Table 2. Calculated Enthalpy and Entropy. (Enthalpy and entropy for dissociation of subunits from a cluster, mixing of dissociated subunits, and overall enthalpy and entropy of the process for each adjacent structural level in PY14 and PB15:3 pigment nanoparticles from the fits to $\Delta G_{1(0)}^d$, $\Delta G_{1(0)}^m$ vs T and $\Delta G_{2(1)}^d$, $\Delta G_{2(1)}^m$ vs T in Figures 4 and 5, respectively^a)

	ΔH^d (kJ/mol _s)	ΔS^d (J/(mol _s K))	ΔH^m (kJ/mol _s)	ΔS^m (J/(mol _s K))	ΔH (kJ/mol _s)	ΔS (J/(mol _s K))
PY14						
dissociation of elemental subunits (0) from primaries (1) and subsequent mixing	59 ± 5	126 ± 16	30 ± 2	42 ± 8	29 ± 5	84 ± 18
dissociation of primary subunits (1) from aggregates (2) and subsequent mixing	-37 ± 7	-208 ± 24	-19 ± 4	-125 ± 12	-18 ± 8	-83 ± 27
PB15:3						
dissociation of elemental subunits (0) from primaries (1) and subsequent mixing	63 ± 2	139 ± 7	35 ± 3	58 ± 10	28 ± 4	81 ± 12
dissociation of primary subunits (1) from aggregates (2) and subsequent mixing	-34 ± 8	-201 ± 26	-17 ± 4	-122 ± 13	-17 ± 9	-79 ± 29

^aNote that mol_s indicates moles of subunits.

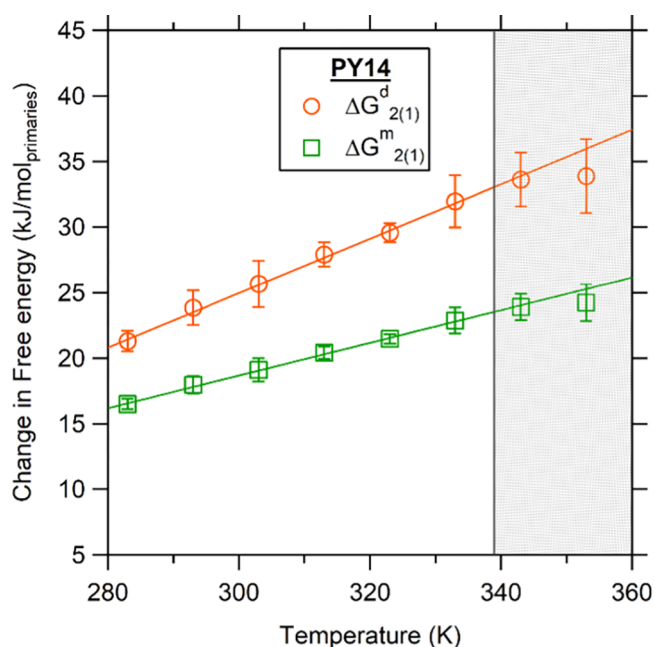


Figure 5. Change in free energy vs T for the aggregate structural level ($i = 2$) for the dilute sample of PY14 across the temperature range from 283 to 353 K. The change in free energy upon dissociation of a primary particle from an aggregate (orange circles) and the change in free energy upon mixing of the primary particle into the dispersing medium (green squares) are plotted. Since the change in the free energy upon dissociation is higher than the change in the free energy upon mixing, the overall change in free energy for the removal of a primary particle from an aggregate is positive. This is consistent with the observation of aggregates. The gray line corresponds to the cloud point of the surfactant (339 K), and the values for $\Delta G_{2(1)}^d$ and $\Delta G_{2(1)}^m$ in the temperature range corresponding to phase separation of pigment from the solution (gray shaded region) are outliers to the dissociation (orange) and mixing (green) fit lines. The plot of the change in free energy vs T at this structural level ($i = 2$) for PB15:3 is shown in Figure S3 in the Supporting Information.

observed to increase with temperature, $\Delta G_{2(1)}$ is predicted to increase with temperature following eq 2. This suggests that the change in entropy for removing a primary particle from an aggregate is negative. A similar dependence of $\Delta G_{2(1)}^d$ and $\Delta G_{2(1)}^m$ over the entire temperature range is also observed for PB15:3 primary particles, as shown in Figure S3 in the Supporting Information.

Figure 6. Overall change in free energy ($\Delta G_{i(i-1)}^d - \Delta G_{i(i-1)}^m$) for the process of removing an elemental subunit

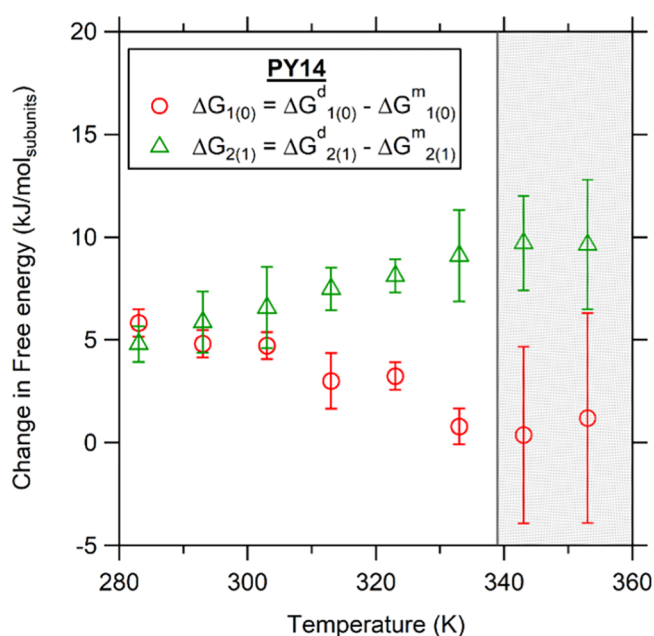


Figure 6. Overall change in free energy upon the removal of an elemental subunit from a primary particle (red circles) vs T for the primary particle structural level ($i = 1$) and the overall change in free energy upon the removal of a primary particle from an aggregate (green triangles) vs T for the aggregate structural level ($i = 2$) for the dilute sample of PY14 across the temperature range from 283 to 353 K. $\Delta G_{1(0)}$ and $\Delta G_{2(1)}$ are calculated using eq 6. The vertical line corresponds to the cloud point of the surfactant (339 K), and the experimental temperature range corresponding to phase separation of pigment from the solution is shaded. The overall change in free energy for the removal of a subunit from a structural level ($i > 0$) for PB15:3 is shown in Figure S4 in the Supporting Information.

from a primary particle ($i = 1$) and removal of a primary particle from an aggregate ($i = 2$) for PY14. The change in free energy required to remove an elemental subunit from a primary particle decreases across the temperature series. Although the energy cost to remove an elemental subunit from a primary particle is decreased at elevated temperatures, one should note that removing an elemental subunit is still an unfavorable process at temperatures below the cloud point of the Triton X-100 surfactant. Furthermore, the positive $\Delta G_{1(0)}$

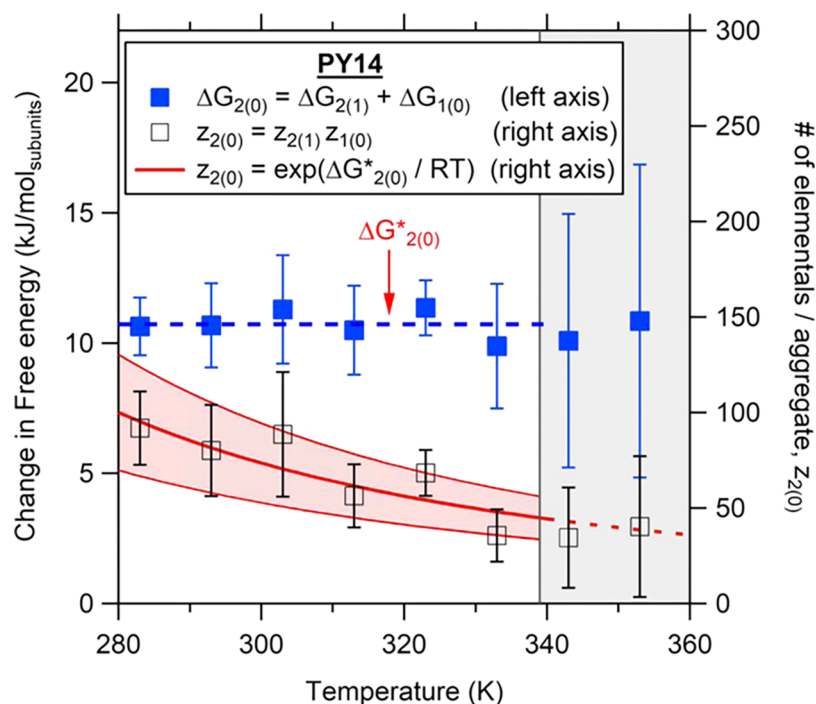


Figure 7. Overall change in free energy, $\Delta G_{2(0)} = \Delta G_{2(1)} + \Delta G_{1(0)}$ (blue solid squares, left axis), upon the removal of an elemental crystallite from an aggregate vs T for the aggregate structural level ($i = 2$) for the dilute sample of PY14 across the temperature range from 283 to 353 K. The average overall change in free energy, $\Delta G_{2(0)}^*$, from 283 to 339 K is 11 ± 0.7 kJ/mol_{elementals} (blue dotted line, left axis). Comparison of average number of elementals per aggregate, $z_{2(0)} = \exp(\Delta G_{2(0)}^*/RT)$ (red solid line, right axis), from eq 2 with $z_{2(0)} = z_{2(1)}z_{1(0)}$ (black open squares, right axis) as a function of temperature. Note that the red shaded region accounts for the error in the estimate of $z_{2(0)}$ from $\Delta G_{2(0)}^*$. The gray line corresponds to the cloud point of the surfactant (339 K), and the experimental temperature range corresponding to phase separation of pigment from the solution is shaded. The overall change in free energy upon the removal of an elemental crystallite from an aggregate vs T and an estimate of the average number of elementals per aggregate from the total change in free energy for PB15:3 is shown in Figure S5 in the Supporting Information.

is consistent with the observation of primary particles in the sample since a negative change in free energy required for an elemental subunit removal would suggest spontaneous breakage of the primary particle into free elemental particles. $\Delta G_{1(0)}$ has a positive entropy change indicating normal breakup of elementals from the primary particle to make a disordered dispersion. In the same vein, a positive value of $\Delta G_{2(1)}$ is consistent with the observation of aggregates and is expected based on the analysis of the small-angle scattering data for PY14 in the series of temperature measurements. Although the process is energetically unfavorable, this result is expected since aggregates of pigment primary particles are observed. Contrary to $\Delta G_{1(0)}$, $\Delta G_{2(1)}$ has a negative entropy change. This might be explained using the hydrophobic effect, that is, upon the removal of a primary from an aggregate, water might organize around the primary particle leading to a reduction in the entropy of the system.³⁴ The trends in $\Delta G_{1(0)}$ and $\Delta G_{2(1)}$ in Figure 6 are consistent with the variation in the average number of primary particles in an aggregate and the average number of elemental particles in a primary particle with temperature. Similar trends for PB15:3 in the overall change in free energy, $\Delta G_{1(0)}$ and $\Delta G_{2(1)}$, with increasing temperature are shown in Figure S4 in the Supporting Information.

Figure 7 shows the overall change in free energy ($\Delta G_{2(0)}$) for the process of removing an elemental subunit from an aggregate ($i = 2$) of PY14. $\Delta G_{2(0)}$ was estimated from the sum of the changes in free energy for adjacent structural hierarchies, $\Delta G_{2(1)}$ and $\Delta G_{1(0)}$, and can be read from the left axis. $\Delta G_{2(0)}$ seems to be a constant with an average value of 11 ± 0.7 kJ/

mol_{elementals} over the temperature range until the cloud point (at 339 K) of the surfactant, beyond which a slight deviation is observed. The same result can also be inferred from Table 2 since the overall change in entropy for the dissociation and mixing of sub-subunits (elementals) from aggregates, $\Delta S_{2(0)} = \Delta S_{1(0)} + \Delta S_{2(1)} \approx 0$. The average value, $\Delta G_{2(0)}^*$, was used to estimate the average number of elemental crystallites per aggregate, $z_{2(0)} = \exp(\Delta G_{2(0)}^*/RT)$, from eq 2, over the temperature range and can be read from the right axis. Note that the red shaded region indicates the error in the estimate of $z_{2(0)}$. This estimate was compared to the actual average number of elementals per aggregate, $z_{2(0)} = z_{2(1)}z_{1(0)}$, and can be read from the right axis in Figure 7. The two approaches yield similar results within error with increasing temperature until the cloud point of the surfactant (339 K). This confirms that the thermodynamics of dissociation and subsequent mixing of sub-subunits at a higher structural level can be ascertained if the average number of subunits at each adjacent structural level over a temperature series is known. A roughly constant value of $\Delta G_{2(0)}$ indicates an exponential decay in aggregate mass, $z_{2(0)}$, with increasing temperature from eq 2. This result combined with the trends in $z_{2(1)}$ and $z_{1(0)}$ shown in Figure 2 indicates that the aggregates grow at the expense of the primary particles and the ink is expected to be composed of larger aggregates with smaller primary particles and more free elementals with increasing temperature. A similar result is observed for PB15:3 pigment nanoparticles as shown in Figure S5 in the Supporting Information, wherein the reduction in

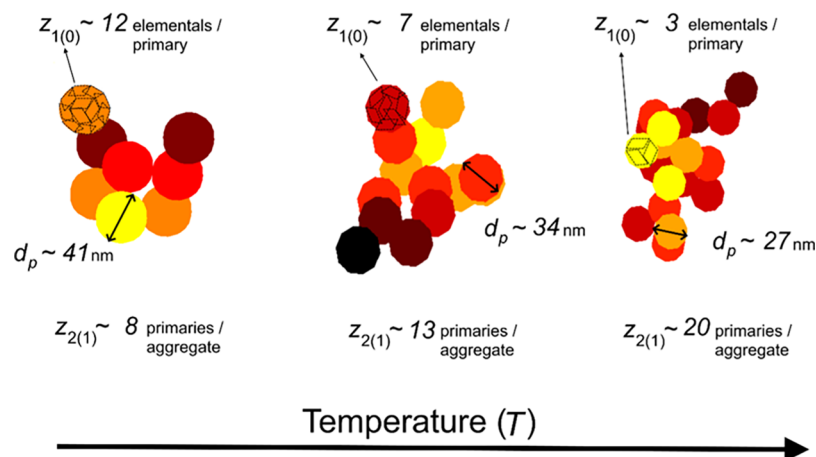


Figure 8. Rearrangement of simulated²⁶ nanoparticle pigment PY14 aggregates with increasing temperature. At higher temperatures, the overall change in free energy to remove an elemental crystallite from a primary particle is decreased. Simultaneously, the overall change in free energy to remove a primary particle from an aggregate is increased across the temperature series. The total aggregate mass (proportional to the number of elemental particles in an aggregate) is observed to reduce with temperature as the aggregates rearrange to form new equilibrium fractal structures.

$z_{2(0)}$ with increasing temperature follows the slight deviation in $\Delta G_{2(0)}$ within error.

For both pigment yellow 14 and pigment blue 15:3, positive $\Delta G_{1(0)}$, positive $\Delta G_{2(1)}$, positive $\Delta S_{1(0)}$, and negative $\Delta S_{2(1)}$ for the removal of subunits are calculated. This suggests a rearrangement of the aggregates to increase $z_{2(1)}$ at the expense of primary particle size, $z_{1(0)}$, with increasing temperature as mentioned in Table 1. Furthermore, the exponential decrease with temperature in aggregate mass, $z_{2(0)}$, indicates that the rearrangement predicted above applies such that additional elemental crystallites are removed from both PY14 and PB15:3 aggregates. Combining these results, Figure 8 depicts the rearrangement of the pigment nanoparticle aggregates with increasing temperature for PY14. These aggregate structures were simulated using scattering structural data and the code provided by Mulderig et al.²⁶

In this work, an attempt was made to determine the thermodynamic behavior of the structural hierarchy of the PY14 and PB15:3 nanoparticles in thermal equilibrium for the primary particles (structural level $i = 1$) and the aggregates (structural level $i = 2$). Although tertiary particles (agglomerates) were not investigated, the theory developed by Vogtt should be applicable to higher structural levels in hierarchical materials if they exist at thermal equilibrium.²³

CONCLUSIONS

The thermodynamics of reversible aggregation was investigated for surfactant-stabilized fractal nanoparticles dispersed in an aqueous solution. A marked decrease in primary particle size (and aggregate size) was observed in the USAXS and SAXS measurements with increasing temperature as the cloud point for the surfactant was approached. The affinity of the surfactant for the surface of the pigment particles increases as its solubility decreases with temperature. Since the organic pigments are soft aggregates, the nanoparticle aggregates are able to break apart and rearrange to form equilibrium structures for each temperature. The Scherrer equation was used to determine that the primary particles were polycrystalline and composed of elemental crystallites that could reversibly dissociate or associate with the primary particles for both PY14 and PB15:3. As the temperature increased

across the series, the aggregate mass was observed to decrease for PB15:3, but it stayed constant for PY14. However, both pigments showed the dissociation of elemental subunits from the primary particles reducing the primary particle size. The degree of aggregation increased due to the increased surface area of the primary particles with higher temperature. Using the theory developed by Vogtt, the change in free energy of dissociation and the change in free energy of mixing were calculated and compared for each structural hierarchical level. The energy barrier for dissociation of elemental subunits was observed to decrease with temperature until the cloud point of the surfactant. However, the energy barrier to remove an elemental subunit from a secondary particle (aggregate) was determined to be positive and relatively constant across the temperature range. The positive energy barrier to elemental particle dissociation is consistent with the observation of nanoparticle aggregates in the pigment-based inks.

A new approach to calculating the free energy of nanoaggregates is demonstrated for these pigment aggregates. The model allows predictive control over nanoaggregate structure through the modification of the surfactant, control of temperature, and modification of the surfactant miscibility through a change in surfactant solubility due to the addition of additives, although the application may be limited when various types of organic and inorganic pigments are used. The thermal control of pigment structure could prove to be a useful tool for the design of pigments for numerous applications.

ASSOCIATED CONTENT

Supporting Information

The Supporting Information is available free of charge on the ACS Publications website at DOI: 10.1021/acs.langmuir.9b02192.

Derivations of eqs 4–6 following the Vogtt model;²³ Unified Fit parameters at varying temperatures for dilute PY14 and PB15:3 inks; temperature dependence of $z_{1(0)}$ and $z_{2(1)}$, change in free energies of dissociation ($\Delta G_{1(0)}^d$ and $\Delta G_{2(1)}^d$), mixing ($\Delta G_{1(0)}^m$ and $\Delta G_{2(1)}^m$), overall free-energy change ($\Delta G_{1(0)}$ and $\Delta G_{2(1)}$), overall change in free energy of combined structural levels, $\Delta G_{2(0)}$, and predicted $z_{2(0)}$ for PB15:3 inks (PDF)

■ AUTHOR INFORMATION

Corresponding Author

*E-mail: gbeaucage@gmail.com. Phone: +1 (513) 556 3063.

ORCID 

Kabir Rishi: 0000-0002-3159-031X

Gregory Beaucage: 0000-0002-6632-0889

Karsten Vogtt: 0000-0003-3206-1070

Author Contributions

Equal contribution by K.R and A.M.

Notes

The authors declare no competing financial interest.

■ ACKNOWLEDGMENTS

This material is based upon the work supported by the National Science Foundation under Grant No. 1635865. Andrew Mulderig was supported by the Department of Energy through the DOE Office of Science Graduate Student Research Program. The use of the Advanced Photon Source, an Office of Science User Facility operated for the U.S. Department of Energy (DOE) Office of Science by Argonne National Laboratory, was supported by the U.S. DOE under Contract No. DE-AC02-06CH11357. USAXS data was collected at the Advanced Photon Source on beamline 9-ID-C operated by the X-ray Science Division. The authors gratefully acknowledge the vital assistance of Jan Ilavsky and his staff at 9-ID-C.

■ REFERENCES

- Pratsinis, S. E. Flame Aerosol Synthesis of Ceramic Powders. *Prog. Energy Combust. Sci.* **1998**, *24*, 197–219.
- Schaefer, D. W.; Hurd, A. J. Growth and Structure of Combustion Aerosols: Fumed Silica. *Aerosol Sci. Technol.* **1990**, *12*, 876–890.
- Schaefer, D. W.; Olivier, B. J.; Hurd, A. J.; Beaucage, G. B.; Ivie, J. J.; Herd, C. R. Structure of Combustion Aerosols. *J. Aerosol Sci.* **1991**, *22*, S447–S450.
- Jin, Y.; Beaucage, G.; Vogtt, K.; Jiang, H.; Kuppa, V.; Kim, J.; Ilavsky, J.; Rackaitis, M.; Mulderig, A.; Rishi, K.; Narayanan, V. A Pseudo-Thermodynamic Description of Dispersion for Nanocomposites. *Polymer* **2017**, *129*, 32–43.
- Rishi, K.; Beaucage, G.; Kuppa, V.; Mulderig, A.; Narayanan, V.; McGlasson, A.; Rackaitis, M.; Ilavsky, J. Impact of an Emergent Hierarchical Filler Network on Nanocomposite Dynamics. *Macromolecules* **2018**, *51*, 7893–7904.
- Skillas, G.; Agashe, N.; Kohls, D. J.; Ilavsky, J.; Jemian, P.; Clapp, L.; Schwartz, R. J.; Beaucage, G. Relation of the Fractal Structure of Organic Pigments to Their Performance. *J. Appl. Phys.* **2002**, *91*, 6120–6124.
- Mather, R. R. The Degree of Crystal Aggregation in Organic Pigments. *Dyes Pigm.* **1999**, *42*, 103–106.
- Faulkner, E.; Schwartz, R. *High Performance Pigments*; Wiley-VCH Verlag GmbH & Co. KGaA: Weinheim, Germany, 2009.
- Beaucage, G.; Kammler, H. K.; Pratsinis, S. E. Particle Size Distributions from Small-Angle Scattering Using Global Scattering Functions. *J. Appl. Crystallogr.* **2004**, *37*, S23–S35.
- Barrow, M. The Crystal and Molecular Structures of Three Diarylide Yellow Pigments, C. I. Pigments Yellow 13, 14 and 63. *Dyes Pigm.* **2002**, *55*, 79–89.
- Schmidt, M. U.; Dinnebier, R. E.; Kalkhof, H. Crystal Engineering on Industrial Diaryl Pigments Using Lattice Energy Minimizations and X-Ray Powder Diffraction. *J. Phys. Chem. B* **2007**, *111*, 9722–9732.
- Sharp, J. H.; Abkowitz, M. Dimeric Structure of a Copper Phthalocyanine Polymorph. *J. Phys. Chem. A* **1973**, *77*, 477–481.
- Robertson, J. M. 136. An X-Ray Study of the Structure of the Phthalocyanines. Part I. The Metal-Free, Nickel, Copper, and Platinum Compounds. *J. Chem. Soc.* **1935**, *0*, 615.
- Beaucage, G. Approximations Leading to a Unified Exponential/Power-Law Approach to Small-Angle Scattering. *J. Appl. Crystallogr.* **1995**, *28*, 717–728.
- Beaucage, G. Small-Angle Scattering from Polymeric Mass Fractals of Arbitrary Mass-Fractal Dimension. *J. Appl. Crystallogr.* **1996**, *29*, 134–146.
- Schaefer, D. W.; Martin, J. E.; Wiltzius, P.; Cannell, D. S. Fractal Geometry of Colloidal Aggregates. *Phys. Rev. Lett.* **1984**, *52*, 2371–2374.
- Scherrer, P. Bestimmung Der Gröss Kolloidteilchen Mittels Röntgenstrahlen *Nachrichten von der Gesellschaft der Wissenschaften zu Göttingen, Math. Klasse* **1918**, *2*, 98–100.
- Patterson, A. L. The Scherrer Formula for X-Ray Particle Size Determination. *Phys. Rev.* **1939**, *56*, 978–982.
- Cullity, B. D. *Elements of X-ray Diffraction*; Addison-Wesley: Reading, MA, 1956.
- Kammler, H. K.; Beaucage, G.; Mueller, R.; Pratsinis, S. E. Structure of Flame-Made Silica Nanoparticles by Ultra-Small-Angle X-Ray Scattering. *Langmuir* **2004**, *20*, 1915–1921.
- Dong, J.; Chen, S.; Corti, D. S.; Franses, E. I.; Zhao, Y.; Ng, H. T.; Hanson, E. Effect of Triton X-100 on the Stability of Aqueous Dispersions of Copper Phthalocyanine Pigment Nanoparticles. *J. Colloid Interface Sci.* **2011**, *362*, 33–41.
- Yang, Y.-J.; Corti, D. S.; Franses, E. I. Effect of Triton X-100 on the Stability of Titania Nanoparticles against Agglomeration and Sedimentation: A Masked Depletion Interaction. *Colloids Surf., A* **2017**, *516*, 296–304.
- Vogtt, K.; Beaucage, G.; Rishi, K.; Jiang, H.; Mulderig, A. Hierarchical Approach to Aggregate Equilibria, Submitted to Physical Review Research.
- Beaucage, G. Determination of Branch Fraction and Minimum Dimension of Mass-Fractal Aggregates. *Phys. Rev. E* **2004**, *70*, No. 031401.
- Rai, D. K.; Beaucage, G.; Jonah, E. O.; Britton, D. T.; Sukumaran, S.; Chopra, S.; Gonfa, G. G.; Härting, M. Quantitative Investigations of Aggregate Systems. *J. Chem. Phys.* **2012**, *137*, No. 044311.
- Mulderig, A.; Beaucage, G.; Vogtt, K.; Jiang, H.; Kuppa, V. Quantification of Branching in Fumed Silica. *J. Aerosol Sci.* **2017**, *109*, 28–37.
- Cates, M. E.; Candau, S. J. Statics and Dynamics of Worm-like Surfactant Micelles. *J. Phys.: Condens. Matter* **1990**, *2*, 6869–6892.
- Vogtt, K.; Beaucage, G.; Weaver, M.; Jiang, H. Thermodynamic Stability of Worm-like Micelle Solutions. *Soft Matter* **2017**, *13*, 6068–6078.
- Ilavsky, J.; Jemian, P. R.; Allen, A. J.; Zhang, F.; Levine, L. E.; Long, G. G. Ultra-Small-Angle X-Ray Scattering at the Advanced Photon Source. *J. Appl. Crystallogr.* **2009**, *42*, 469–479.
- Ilavsky, J.; Zhang, F.; Allen, A. J.; Levine, L. E.; Jemian, P. R.; Long, G. G. Ultra-Small-Angle X-Ray Scattering Instrument at the Advanced Photon Source: History, Recent Development, and Current Status. *Metall. Mater. Trans. A* **2013**, *44*, 68–76.
- Ilavsky, J.; Jemian, P. R. Irena: Tool Suite for Modeling and Analysis of Small-Angle Scattering. *J. Appl. Crystallogr.* **2009**, *42*, 347–353.
- Mulderig, A.; Beaucage, G.; Vogtt, K.; Jiang, H.; Jin, Y.; Clapp, L.; Henderson, D. C. Structural Emergence in Particle Dispersions. *Langmuir* **2017**, *33*, 14029–14037.
- Akbaş, H.; Boz, M.; Batıgöç, Ç. Study on Cloud Points of Triton X-100-Cationic Gemini Surfactants Mixtures: A Spectroscopic Approach. *Spectrochim. Acta, Part A* **2010**, *75*, 671–677.
- Tanford, C. *The Hydrophobic Effect: Formation of Micelles and Biological Membranes*, 2nd ed.; John Wiley: New York, 1980.